



1352–2310(94)E0022-C

DEPOSITION OF ATMOSPHERIC PARTICLES WITHIN THE BUDDHIST CAVE TEMPLES AT YUNGANG, CHINA

CHRISTOS S. CHRISTOFOROU, LYNN G. SALMON and GLEN R. CASS*

Mechanical Engineering Department and Environmental Quality Laboratory, California Institute of Technology, Pasadena, CA 91125, U.S.A.

(First received 7 June 1993 and in final form 22 December 1993)

Abstract—The Buddhist cave temples at Yungang, China, are soiled at a rapid rate by the deposition of airborne particles. Average mass deposition rates to horizontal surfaces of $13.42 \mu\text{g m}^{-2} \text{s}^{-1}$ outdoors and $5.23 \mu\text{g m}^{-2} \text{s}^{-1}$ inside Cave 6 were measured over a 1 yr period in 1991–1992. These rates are comparable to the rates inferred by examination of historically accumulated deposits within the caves. The surface area coverage by coarse particles is dominated by particles larger than about $10\text{--}20 \mu\text{m}$ in diameter, while the mass flux is dominated by even larger particles greater than $20\text{--}30 \mu\text{m}$ in diameter. Comparison of the deposition rate in Cave 6, which retains its wooden temple front structure, to that in Cave 9 which is open to the outdoors shows that the temple front does provide some protection. During spring 1991, the deposition rate to horizontal surfaces in Cave 6 was $4.5 \mu\text{g m}^{-2} \text{s}^{-1}$ compared to $13.4 \mu\text{g m}^{-2} \text{s}^{-1}$ in Cave 9 and $21.5 \mu\text{g m}^{-2} \text{s}^{-1}$ outdoors.

Key word index: Airborne particles, dry deposition, soiling, art conservation.

INTRODUCTION

Ancient monuments exposed to the environment are subject to physical, chemical, and biological degradation over the years. This can be caused, for example, by weathering by the elements over time, including factors such as erosion by rainfall, the daily cycling of temperature and relative humidity that produces stresses in stone objects, and by freeze/thaw cycles. Air pollution and windborne dust can likewise degrade stone sculpture. Airborne particles that deposit onto stone monuments will absorb and scatter light that would otherwise be reflected to an observer and therefore will affect the object's visual qualities (Nazaroff and Cass, 1991). Over time, deposited particles can become incorporated into the surface of the gypsum crusts that form on some types of stone, thereby permanently altering the surface.

One archaeological site that suffers from a very high rate of airborne particle deposition is the collection of more than 20 Buddhist cave temples at Yungang in northern China. The Yungang Grottoes are carved into the side of the Wuzhou hills, about 16 km west of the industrial city of Datong, in the north of Shanxi province. The earliest caves were excavated into the face of a sandstone cliff under the patronage of the emperors of the Northern Wei Dynasty (Knauer, 1983) during the middle of the 5th century A. D. Many of the caves consist of an interior chamber approxi-

ately 12 m by 12 m by 15 m high, hollowed out around a central column about 10 m high that typically is carved into a monumental statue of the Buddha. More than 50,000 smaller Buddhist carvings adorn the interior walls of the caves, and depict scenes from the life of the Buddha. In antiquity, the entrances to each large cave were covered by a wooden temple front several storeys high and one room deep. Significant repairs to the caves were made during the 11th and 17th centuries. By the early 20th century, travelers to the area report that the caves had fallen into a state of neglect (Cox, 1957). In more recent years the caves have been cleaned, and their surroundings turned into a park. Hundreds of visitors visit the site daily.

Today, Yungang is surrounded by one of China's largest coal mining regions. Particles are generated by the various processes at the mines. Coal truck traffic on nearby highways produces much dust. Coal combustion occurs for cooking and heating in the village of Yungang. Coal-fired locomotives run on nearby railroad tracks. Traffic on dirt roads in the village of Yungang creates additional dust. Since Yungang is located near the edge of the Gobi desert, it also is affected by regional dust storms. As a result of a combination of the above, the Yungang Grottoes suffer from a severe soiling problem.

The caves and the carvings inside were cleaned in 1986 and documentary photographs were taken. Today, however, there is visible soiling due to the deposition of airborne particles onto the sculptures, especially on upward-facing horizontal surfaces. During

* To whom all correspondence should be addressed.

the present study the thickness of the particle deposits was measured to be at some places as deep as 0.8 cm at sites that were photographed in a cleaned condition in 1986. The relationship between the ambient particulate air pollution problem and the deposition flux within the caves needs to be established. Knowing the sources that generate particle emissions to the atmosphere, as well as their size distribution, will allow control strategies to be devised and implemented, which in turn will enable the control of the deposition flux of particles onto surfaces in the caves.

During the month of April 1991, an extensive environmental monitoring experiment was conducted at the Yungang Grottoes. The overall purpose of this work was to characterize the exposure of the grottoes to air pollutants in a manner that will establish a basis for the future protection of the grottoes from air pollution damage.

A series of experiments were designed to achieve the following objectives:

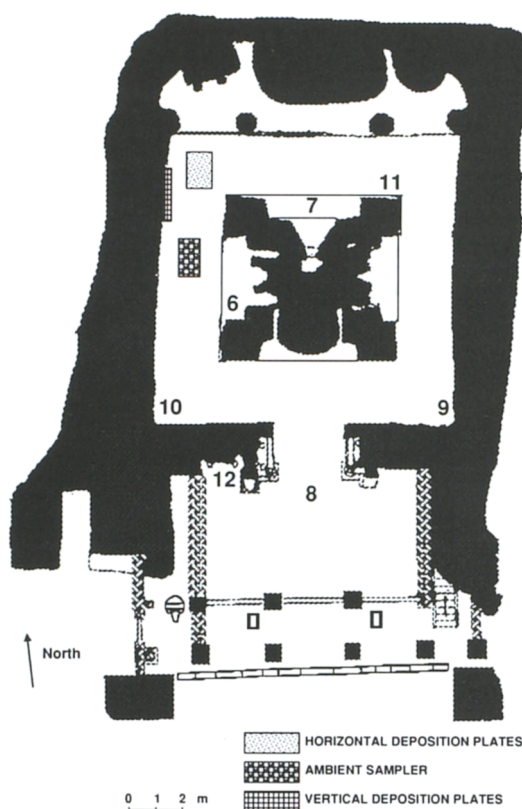
- (1) To determine the airborne particle size distribution necessary for engineering calculations of particle filtration characteristics (which are needed for control system design).
- (2) To measure particle deposition fluxes to both vertical and horizontal surfaces within the caves.
- (3) To measure particle deposition fluxes throughout the community (an area of about 2.0 km by 2.0 km around the site) to help identify the location of the source of the particles.
- (4) To understand the fluid mechanics of air exchange that brings airborne particles into the caves.
- (5) To characterize the concentration and chemical composition of airborne particles and some pollutant gases (e.g. SO₂) both inside and outside the caves.
- (6) To measure the chemical character of local sources of particle release to the atmosphere as a possible means of identifying the presence of material from specific sources within the deposits in the caves.
- (7) To understand how the reconstruction of shelters or temple fronts could be used to help control particle intrusion into the caves.

The present work is primarily concerned with the first two items in the list above.

EXPERIMENTAL METHODS

Sample collection

Two caves were chosen for analysis, Caves 6 and 9. As shown in Figs 1 and 2, their architecture is similar: an elliptic interior shape with a large central pillar, a large entrance at ground level with a smaller opening into the cliff at about the third floor level. Cave 6, unlike Cave 9, still retains its wooden temple front, the surfaces of which consist largely of narrow wooden doors with a wooden lattice work backed by paper windows. Samples were taken inside Cave 6, inside Cave 9, and under the overhanging cliff outside Cave 9, at locations shown in Figs 1 and 2.



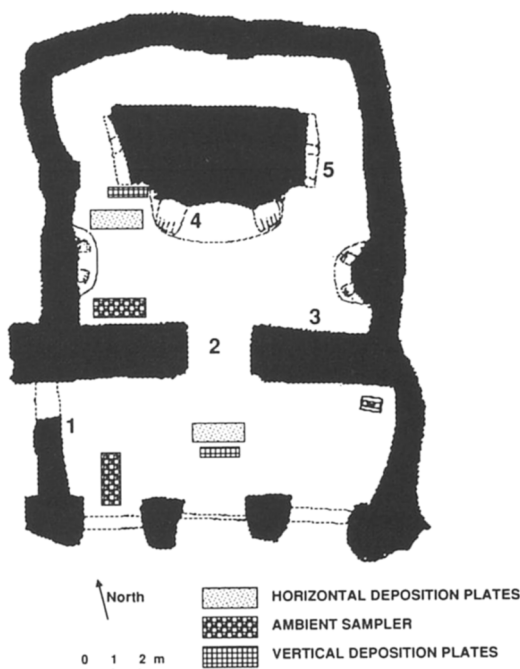
CAVE 6 – LOCATIONS OF DUST DEPOSIT SAMPLES

Fig. 1. Horizontal section of Cave 6 showing ambient sampler and deposition plates location. The numbers show the location of the measurements of accumulated deposits from the period 1986–1991 (see Table 4).

Both long- and short-term experiments were carried out. During the spring of 1991, eight 24 h periods were sampled, beginning at midnight of 12, 14, 17, 20, 23, 26, 29 April and 1 May (first sampling period). The results from this sampling program will be used to characterize the concentration and size distribution of airborne coarse particles, as well as deposition patterns of atmospheric coarse particles, over the course of a spring month. A second set of two experiments lasted 48 h each with samples taken over consecutive 4 h intensive sampling periods. These two intensive periods began at 2:00 a.m. on 15 April, and at 2:00 a.m. on 24 April. The results from the two intensive periods will be used at a later point to provide model validation data to a theoretical model that predicts particle deposition patterns within the caves, given the atmospheric concentration.

In order to better understand particle concentration and deposition patterns and how they are affected by seasonal variations, the sampling program was continued. Samples of 24 h duration were taken at 6-d intervals during one month of each remaining quarter of the year (July 1991; October 1991; January 1992). During these three sampling periods, deposition measurements were made at two of the three locations sampled during the spring of 1991: inside Cave 6 and outdoors. Sampling for the characterization of the aerosol concentration and size distribution at the two sites also was continued.

During the spring sampling period, the deposition flux to both horizontal and vertical surfaces was measured at each of the three locations. The objective of these experiments was to measure the flux to surfaces of coarse particles greater than 2.1 μm diameter. Coarse particle deposition to horizontal



CAVE 9 – LOCATIONS OF DUST DEPOSIT SAMPLES

Fig. 2. Horizontal section of Cave 9 showing ambient sampler and deposition plates location. The numbers show the location of the measurements of accumulated deposits from the period 1986–1991 (see Table 4).

surfaces occurs at a relatively rapid rate by inertial deposition mechanisms and by gravitational sedimentation. Deposition to vertical surfaces is much slower because gravitational sedimentation acts parallel to the collection surface. In the case of vertical collection surfaces, particle deposition could be significantly affected by turbulent deposition from the convective boundary layer along the cave wall; for the smallest particles of interest to us, thermophoretic motion of the particles driven by temperature differences between the cave walls and the air in the caves could be important (Nazaroff and Cass, 1989a). For that reason, care was taken to bring the vertical deposition plates within the caves to the temperature of the cave walls. The vertical collection plates were fastened on a large aluminum plate which was then held against the cave wall by metal pins such that these plates were in thermal contact with the cave walls. The wall sampled inside Cave 9 was smooth while the wall in Cave 6 was uneven and care was taken to orient the plates such that they were truly vertical as measured by a spirit level. The thermal environment of the horizontal deposition plates is not as important because particle sedimentation dominates the deposition flux in this case. The horizontal deposition plates were placed on top of large wooden platforms about 1 m above ground level. The vertical outdoor deposition surfaces were fastened to an aluminum plate that was then attached to the side of the wooden support that also held the outdoor horizontal collection plates.

As mentioned previously, the cave walls contain both areas with smooth surfaces and areas with rough surfaces. The rough surfaces in turn vary greatly from sand grain-scale roughness elements to areas of decayed rock with irregularities on the scale of centimeters. It is not practical to measure deposition to the rough surfaces using surrogate surfaces, as many roughness scales are involved. Instead, direct observations of historical dust deposits that have

accumulated on the actual rough surfaces should be made in those cases. For the case of the smooth surfaces inside the caves, deposition measurements using surrogate surfaces are practical and were made during the present sampling campaign. Two surrogate surfaces were used for the collection of particles: glass slides (75 mm by 25 mm by 1 mm thick) and Millipore filters (47 mm in diameter, 0.22 μm pore size, membrane filter GSWP047 00). In the case of horizontal plates located inside the caves, where sedimentation toward the plates is the dominant collection mechanism and where high air velocities that might otherwise resuspend deposited particles are not present, particles collected on these surrogate surfaces will reasonably represent collection on most actual horizontal surfaces. For the case of vertically oriented surfaces inside the caves and those surfaces exposed to outdoor wind conditions, these smooth surfaces should adequately simulate actual smooth surfaces, but may collect and retain fewer particles than would be the case for rougher surfaces.

Separate horizontal collection plates were exposed for each of the 24 h periods listed previously, while a single set of vertical deposition plates was continuously exposed for the entire 19-d spring experiment because of the great difference in deposition rates between horizontal and vertical surfaces (Ligocki *et al.*, 1990). Duplicate samples were taken. One of each pair of glass slides was transported back to the laboratory in Pasadena, CA, covered with a thin microscope cover slide (24 mm by 50 mm by 0.15 mm thick) to prevent particles from becoming detached from the surface, while the second slide of each pair was carried carefully but without a cover slip. Only those samples protected by a glass cover slip were used in subsequent analyses. All Millipore filter samples were transported back to the laboratory sandwiched between two glass slides (75 mm by 50 mm by 1 mm thick for the lower plate and 50 mm by 43 mm by 0.15 mm thick for the upper plate). Both glass slides and Millipore filters were transported while secured to the bottom of square covered plastic Petri dishes (100 mm by 100 mm) that were sealed at the edges with Teflon tape. Duplicate samples (only glass slides were used) were collected during the summer, fall, and winter sampling periods and those were sent by courier and air express to the laboratory in Pasadena.

The ambient aerosol samples were taken over 24 h periods by drawing air at a rate of 1 $\ell\text{ min}^{-1}$ through a 47 mm diameter Millipore filter (0.22 μm pore size, membrane filter GSWP047 00) secured in an open-faced filter holder, thus ensuring collection of both large and small particles. The 0.22 μm pore size filter was chosen because the pores are small enough to preclude any loss of larger particles inside the pores. Also, because the pores are small they are invisible under the light microscope (at the magnification used) and therefore do not interfere with particle counting and sizing. The ambient filters were transported back to the laboratory sandwiched between two glass plates and were analysed using optical microscopy. Samples also were taken to determine particle chemical composition in two size ranges, fine ($d_p < 2.1 \mu\text{m}$) and coarse ($d_p > 2.1 \mu\text{m}$). These results are described elsewhere (Salmon *et al.*, 1994). Of importance to the present work, ambient aerosol mass concentration was also determined gravimetrically as part of that further measurement program by pre-weighing and post-weighing of aerosol samples collected on 47 mm diameter Teflon filters. Results of that atmospheric sampling program show that over 74% of the outdoor airborne particle mass at Yungang is in the coarse particle fraction (Salmon *et al.*, 1994), and for that reason the present study focuses on coarse particle deposition.

Optical microscopy analysis

The method used for obtaining the particle size distributions and number counts consists of a light microscope connected to a Macintosh IIci computer via a video camera

Table 1. Comparison of automated micro-video measurements of the diameters of glass microspheres vs measurements made from polaroid photographs

Nominal diameter (μm)	Micro-video high magn. (μm)	Micro-video low magn. (μm)	Polaroid high magn. (μm)	Polaroid low magn. (μm)
40	42.7	42.9	40.6	41.0
40	41.5	41.4	39.6	39.8
40	40.5	40.4	39.3	39.0
20	23.7	22.8	24.1	22.9
20	22.9	21.9	22.5	21.8
20	23.1	21.6	23.1	22.2
11	13.4	—	13.7	—
11	13.6	—	13.8	—

and a special frame-grabbing board (QuickCapture, part No. DT2255, Data Translation, Inc., Marlboro, MA). The deposition sample is placed under the microscope and, with the aid of a public domain analysis program called IMAGE,* a digital picture of the sample is grabbed and stored on the computer for subsequent analysis. A total of 60 video frames are captured per glass slide examined, 30 at $170\times$ magnification (used to size and count particles less than about $18\ \mu\text{m}$) and 30 at $85\times$ magnification (used to size and count particles greater than about $18\ \mu\text{m}$). Each frame in turn must have its background gray-level subtracted, sharpness enhanced, and the lowest gray-level which indicates the presence of a particle must be chosen. The frame is then made strictly black and white (no grays), where black indicates that a particle is present and white indicates space between particles. The program IMAGE then scans the entire frame, counting and recording the number of picture elements (pixels) contained within each black area. The list of particles is sorted from smallest to largest, the number of particles of each size is found, for each size (in pixels) a diameter is approximated by assuming that the cross-sectional area is circular, and then the corresponding spherical volume is calculated. The particles are gathered into consecutive size bins in order to plot particle size and mass distributions. The total mass of all the particles measured in the small and large particle size range is divided by the surface area of the glass slide corresponding to one frame of the appropriate size and number of such frames processed and by the elapsed time over which the glass slide was exposed to produce a particle mass flux to the slide in units of $\mu\text{g m}^{-2} \text{s}^{-1}$. Calculations showed that counting 600 particles per sample gave size distributions that deviated in number counts in the largest size intervals studied by as much as 27% from the true size distribution, while counting 1500 particles per sample resulted in size distributions in the largest size intervals studied that deviated by less than 8% from the true value. A total of 2000 particles were counted, whenever possible, on each glass slide. Particles were then grouped into eleven equal (on a logarithmic scale) size intervals spanning the size range from 2.0 to $147.9\ \mu\text{m}$ particle diameter.

The absolute size accuracy of the automated micro-video method was examined in the laboratory. Glass microspheres of different nominal sizes were deposited onto glass slides, which were subsequently analysed using the micro-video method. The same frames also were analysed "manually": polaroid photographs were taken through the microscope of the same particles as well as an embedded length scale and the image of the spheres was measured using a vernier caliper. The results of these experiments are shown in Table 1. It was

found that the difference in the diameters between the two methods was always less than 5%.

The reproducibility of the results of the automated micro-video method also was tested. For this purpose, two horizontal glass slides (A and B) were exposed simultaneously, outdoors, for the same period of time. Then, 40 frames were captured from each specimen, and analysed (results A1 and B1). The same video frames were processed a second time through IMAGE to determine if there were important effects of the system operator's intervention in the counting process that occurs when translating from gray scale to black and white images (results A2 and B2). Finally, a new set of 40 video frames was captured from each plate, making sure the locations were different from the first set of pictures, and these frames were analysed as well (results A3 and B3). As shown in Fig. 3, it can be seen that there is close agreement in all six cases.

The ambient coarse particle concentration and size distribution also was measured using automated light microscopy. Each ambient sample collected by filtration onto a Millipore filter was sandwiched between a bottom glass plate (75 mm by 50 mm by 1 mm thick) and a top cover glass plate (43 mm by 50 mm by 0.15 mm thick) to keep it flat. It was then placed under the microscope and particle number counts and size were analysed just as for the deposition plates. Knowing the total exposed surface area of the filter and volume of air passed through, the airborne coarse particle size distribution can be obtained. Knowledge of the size distribution permits the calculation of the particulate mass per unit volume of air if a particle density is assumed.

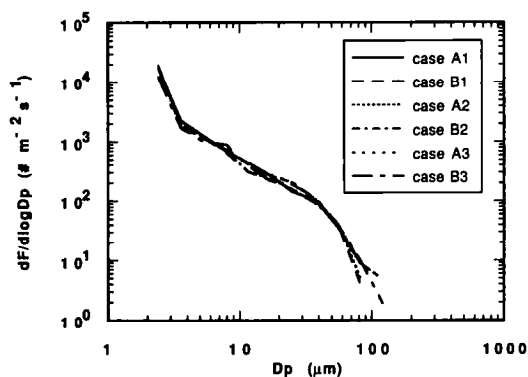


Fig. 3. Reproducibility of the micro-video measurement of the number flux, F , of coarse particulate matter deposited onto two duplicate horizontal slides A and B: case 1 initial imaging and counting; case 2 reprocessing of initial video frames; case 3 second set of video frames taken at different locations on the slides.

* The author is Wayne Rasband and the newest version of the program is available via anonymous ftp from alw.nih.gov or sumex-aim.stanford.edu.

RESULTS AND DISCUSSION

The method of particle size analysis by automated light microscopy has been used by others (Heidenrich, 1987; John *et al.*, 1991), and investigations performed in support of the present study have shown that glass slides are well suited for computer-aided optical microscopy analysis. For that reason the deposition results presented in this study are based on data obtained from glass slides.

Figure 4a shows the average flux of deposited coarse particulate matter onto horizontal surfaces. It represents the average of each of the eight 24 h sampling events during the spring 1991 sampling period. It can be seen that for particle sizes $d_p > 21 \mu\text{m}$, the particle deposition rate outside is higher than in Cave 6, which in turn is higher than inside Cave 9. For particles with $d_p < 21 \mu\text{m}$, however, the particle flux inside Cave 6 and outdoors is about the same. The deposition flux of the smaller ($d_p < 21 \mu\text{m}$) coarse particles inside Cave 9 is higher than at either of the other two locations and that might be due to the fact that the floor in Cave 9 is covered with very soft dirt, unlike Cave 6 which has a tile floor, and the outdoors, where the soil is more heavily packed. Occasional entry into Cave 9, where the control module for our electronic equipment as well as several instruments

was located, may have generated enough dust to have biased the results slightly. It should be noted here that the two largest particle size bins studied were very sparsely populated because the residence time in the atmosphere for particles of that size is very small.

In Figs 4b–d, monthly average particle fluxes outdoors and within Cave 6 are documented for the remaining three seasons of the year. Again, particle deposition rates inside Cave 6 are significantly below those outdoors in all cases except for particles in the 5–30 μm size range during October.

Figure 5 shows the size distribution of coarse airborne particles at each of the three locations during the spring sampling period. Results shown there are the average over all eight 24 h sampling events during the spring 1991 sampling period. It can be seen that for particles larger than 21 μm in diameter, the outdoor concentration is higher than that inside Cave 9, which in turn is higher than that inside Cave 6. That is expected since Cave 6 has the wooden temple front that acts as a partial barrier to the transfer of the coarser particles from the outdoor air to the inside of the cave. As far as the smaller particles are concerned ($d_p < 21 \mu\text{m}$), Fig. 5 suggests no definite trend between the outdoor and indoor sites. That the concentration outdoors is smaller in most size intervals than that inside the caves might be due to the fact that the

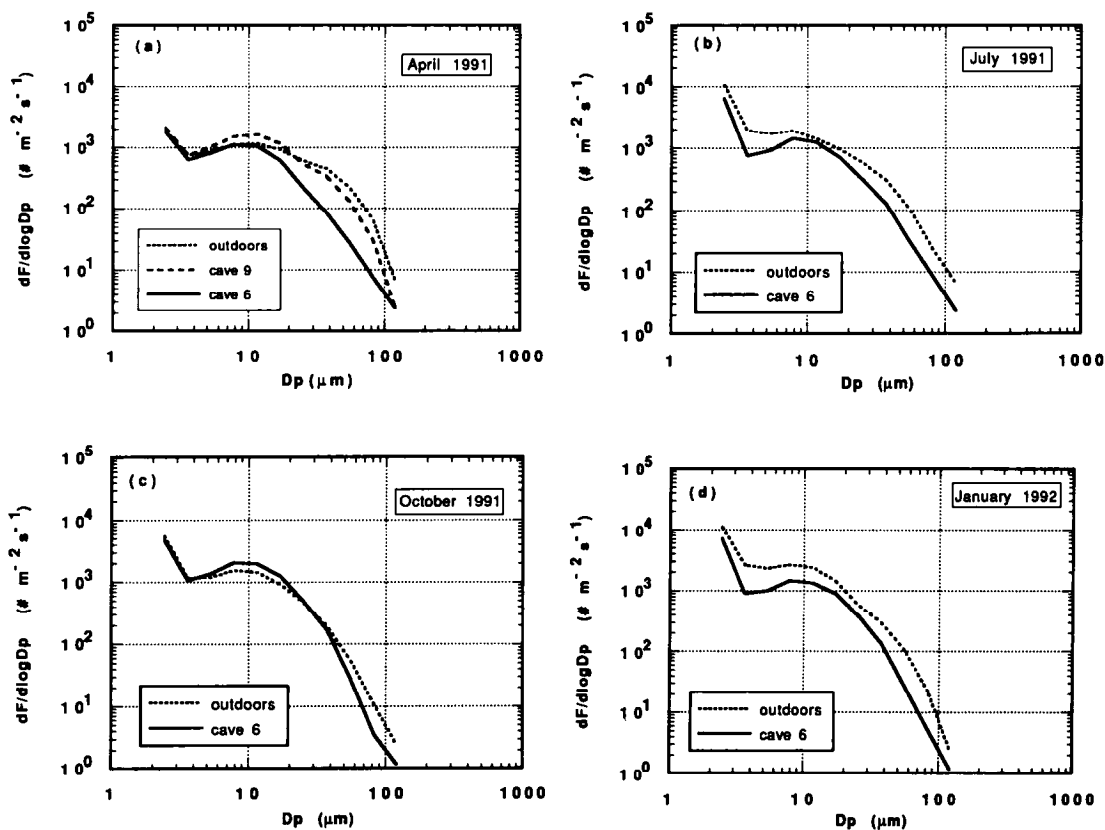


Fig. 4. Average number flux, F , of coarse particulate matter deposited onto horizontal surfaces at Yungang as a function of particle diameter, d_p .

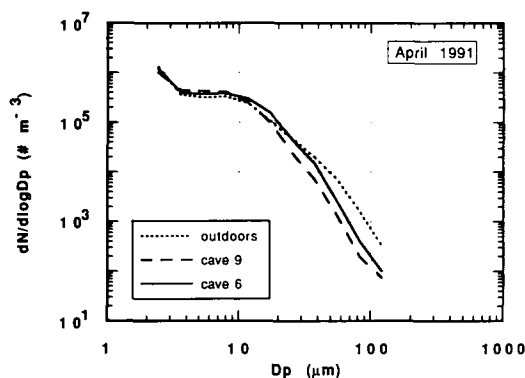


Fig. 5. Average number distribution of coarse airborne particulate matter at Yungang, April 1991, as a function of particle diameter d_p .

visitors to the caves may be a source of dust resuspension.

Table 2 shows the average projected surface area distribution of particles depositing onto horizontal surfaces over all four seasons of the year studied. The projected surface area flux is proportional to the rate at which the surfaces become covered with visible dust. It has been shown that the threshold for human perception that a white surface is becoming soiled by dark-colored particles occurs once about 0.2% of the area of a surface has become covered (Hancock *et al.*, 1976). With brown- or gray-colored particles, a somewhat higher coverage probably would be required before the deposits would become visible. From the data in Table 2, at the deposition coverage rate of $2.9 \times 10^5 \mu\text{m}^2 \text{m}^{-2} \text{s}^{-1}$ observed during the spring within Cave 9, horizontal surfaces would reach 0.2% coverage needed for detectable soiling in about $6.9 \times 10^3 \text{ s}$ or 1.9 h (on average), for example. This is completely consistent with our own observations that the glass plates and millipore filters used in these experiments are noticeably dirty at the end of a day. The surface area coverage tables show that most of the coverage by coarse particles is due to particles in the size range 14–101 μm particle diameter even though smaller particles are more numerous.

The average mass flux to horizontal surfaces is shown in Figs 6a–d. The mass flux was found by integrating the area under the deposited coarse particle number distribution curve, i.e. taking all particles in each size interval to be spheres having a diameter of the same size as the log mid-point of each interval, and finally assuming a density of 2.2 g cm^{-3} for the particles. That particle density value was obtained by measuring the density of a bulk deposit of particles removed from Cave 6. Results from all four seasons of the year are shown. The mass flux to horizontal surfaces inside Cave 6 remains in the range $4.5\text{--}6.2 \mu\text{g m}^{-2} \text{ s}^{-1}$ regardless of the time of the year. Outdoors the mass flux is about the same for summer and winter, but higher during the spring. The lowest

Table 2. Projected surface area flux of coarse particulate matter onto horizontal surfaces at Yungang

Size (μm)	April 1991		July 1991		October 1991		January 1992		
	Outdoors ($\mu\text{m}^2 \text{m}^{-2} \text{s}^{-1}$)	Cave 9 ($\mu\text{m}^2 \text{m}^{-2} \text{s}^{-1}$)	Cave 6 ($\mu\text{m}^2 \text{m}^{-2} \text{s}^{-1}$)	Outdoors ($\mu\text{m}^2 \text{m}^{-2} \text{s}^{-1}$)	Cave 6 ($\mu\text{m}^2 \text{m}^{-2} \text{s}^{-1}$)	Outdoors ($\mu\text{m}^2 \text{m}^{-2} \text{s}^{-1}$)	Cave 6 ($\mu\text{m}^2 \text{m}^{-2} \text{s}^{-1}$)	Outdoors ($\mu\text{m}^2 \text{m}^{-2} \text{s}^{-1}$)	Cave 6 ($\mu\text{m}^2 \text{m}^{-2} \text{s}^{-1}$)
2.02–2.99	1500	1700	1400	8400	5100	3700	8700	5600	1600
3.00–4.42	1300	1300	1100	3400	1300	1800	4500	1600	3800
4.43–6.54	3400	3900	3000	6600	3500	5200	8700	3800	12,000
6.55–9.67	8900	12,200	9200	15,900	12,100	16,800	21,700	24,200	33,400
9.68–14.2	20,900	29,300	18,700	26,200	22,700	35,100	43,100	56,800	87,000
14.3–21.1	35,500	45,300	24,200	38,400	28,700	48,700	56,800	87,000	120,000
21.2–31.2	51,700	65,000	19,100	49,900	27,000	42,000	49,800	87,000	120,000
31.3–46.2	84,800	64,100	16,400	57,100	23,600	36,700	55,800	87,000	120,000
46.3–68.4	91,400	54,100	11,600	42,400	12,500	11,700	43,800	5100	2200
68.5–101.2	60,300	27,800	6800	20,200	7400	3100	20,300	4900	2200
101.3–149.7	13,200	4600	4700	12,300	4500	2600	4900	2200	2200
Total	372,900	289,800	116,200	280,800	148,400	202,700	318,100	160,300	160,300

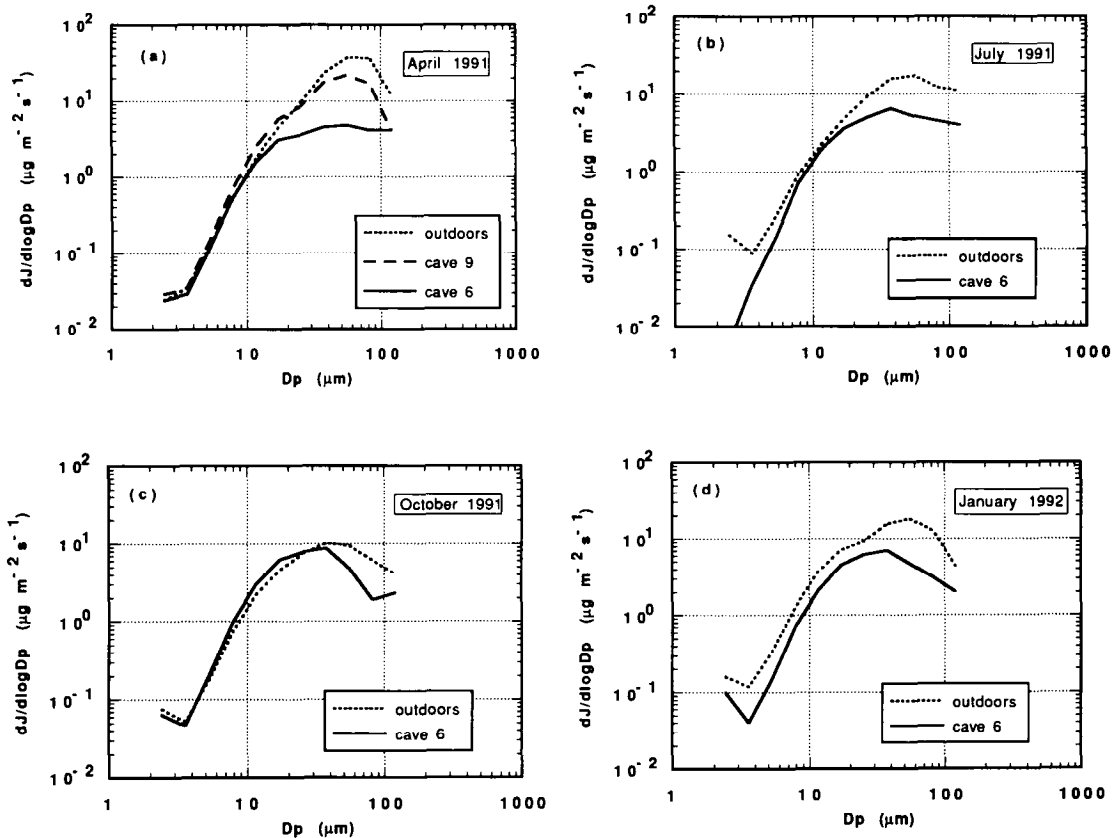


Fig. 6. Average mass flux, J , of coarse particulate matter onto horizontal surfaces at Yungang as a function of particle diameter d_p .

mass fluxes outdoors were found during the fall. The springtime peak in outdoor deposition rates is influenced by regional dust storms that occur at that time of year.

Table 3 shows the total mass flux of coarse particulate matter onto horizontal surfaces. The total mass flux of particulate matter deposited onto horizontal surfaces in Cave 6 is about one-third of that deposited in Cave 9, which in turn is about half the outdoor mass flux.

During the course of the experiment, accumulated deposits were collected from the actual horizontal surfaces of the statues inside Caves 6 and 9, as listed in Table 4, from samples taken at the locations shown in Figs 1 and 2. It was known that those deposits had been accumulating for 5 yr because samples were collected at locations documented in 1986 when selected statues were cleaned during photodocumentation of the grottoes. When the mass deposition rates measured over our year-long experiment are extrapolated to cover the entire period 1986–1991, it is seen that the results of our experiments using surrogate deposition surfaces are comparable to the reality of the deposits on the sculptures (see Table 5).

The particle deposition velocity, which is defined as the ratio of the particle deposition flux ($\text{No. m}^{-2} \text{s}^{-1}$)

to the airborne particle number concentration (No. m^{-3}), is a measure of the fluid mechanical processes that govern particle deposition rates (Ligocki *et al.*, 1990). Theoretical predictions can be made for the deposition velocity under specified air flow conditions (Nazaroff and Cass, 1989a, b). Deposition velocity measurements for coarse particles onto a variety of horizontal surfaces have been reviewed by several authors (e.g. see Nicholson, 1988; Schmel, 1980). Measured results in general do not agree well with theoretically predicted values. During the present study, deposition velocities were computed as a function of particle size by taking the ratio of the particle number flux to the surface to the ambient concentration for each of the particle size intervals defined previously at the three experiment locations. Deposition velocity measurements for 14 April 1991 at Yungang are shown in Fig. 7a. The trend is that of increasing deposition velocity with increasing particle diameter. That is as expected, because the large airborne particles settle out of the atmosphere under the influence of gravity, and the larger the particle the larger its terminal settling velocity. The deposition velocity is shown to be a little larger outdoors than it is inside the two caves but the difference in the deposition velocities in the interior of the two caves is small.

Table 3. Total mass flux onto horizontal surfaces at Yungang

Location	Date	Mass flux ($\mu\text{g m}^{-2} \text{s}^{-1}$)
Outdoors	April 1991	21.50
Inside Cave 9	April 1991	13.40
Inside Cave 6	April 1991	4.54
Outdoors	July 1991	12.70
Inside Cave 6	July 1991	5.43
Outdoors	October 1991	7.16
Inside Cave 6	October 1991	5.84
Outdoors	January 1992	12.30
Inside Cave 6	January 1992	5.12
Outdoors	Annual average	13.42
Inside Cave 6	Annual average	5.23

* Based on a density of $\rho = 2.2 \text{ g cm}^{-3}$.

Table 4. Measurements of accumulated deposits from the period 1986–1991

Site	Location*	Deposit depth (cm)	Mass loading† (g m^{-2})
Outside Cave 9	1	0.76	6658
Cave 9	2	0.25	2695
Cave 9	3	0.06	16‡
Cave 9	4	0.13	572
Cave 9	5	0.8	4981
Cave 6	6	0.13	201
Cave 6	7	0.06	113
Cave 6	8	1.0	2655§
Cave 6	9	0.5	156
Cave 6	10	0.4	171
Cave 6	11	0.5	298
Cave 6	12	0.1	370

* See Figs 1 and 2 for an indication of the various locations.

† Deposits are on horizontal surfaces cleaned in 1986, except for locations 3 and 8.

‡ Deposit on a nearly vertical surface.

§ Deposit on horizontal surface that was not cleaned in 1986.

Table 5. Mass deposition comparison for horizontal surfaces at Yungang

Location	1986–1991 Actual (g m^{-2})*	5-year estimate from glass plate samples (g m^{-2})†
Inside Cave 6	113–370	716
Inside Cave 9	572–4981	2113
Under cliff overhang in front of Cave 9	6658	3390

* Weighed deposit mass collected from a known area.

† Calculated mass deposit using values from Fig. 6, extrapolated to a 5-yr period. Particle density used is $\rho = 2.2 \text{ g cm}^{-3}$.

The experimentally determined deposition velocity values show reasonable agreement to theoretically calculated values of the terminal settling velocity for spherical particles of equivalent volume and density at times when outdoor wind speeds are low, such as during the day shown in Fig. 7a. This calculation depends on the particle density, ρ , and the deposition velocity curves lie close to the terminal settling

velocity curve for $\rho = 2.2 \text{ g cm}^{-3}$. Exact agreement between the deposition velocity for particles to horizontal surfaces in the caves and the terminal settling velocity for a sphere in still air is not expected because the air within the caves is in motion. During the day a downdraft occurs in the caves, while at night an updraft is observed, both circulation patterns being driven by a thermal siphon effect. The outdoor air in

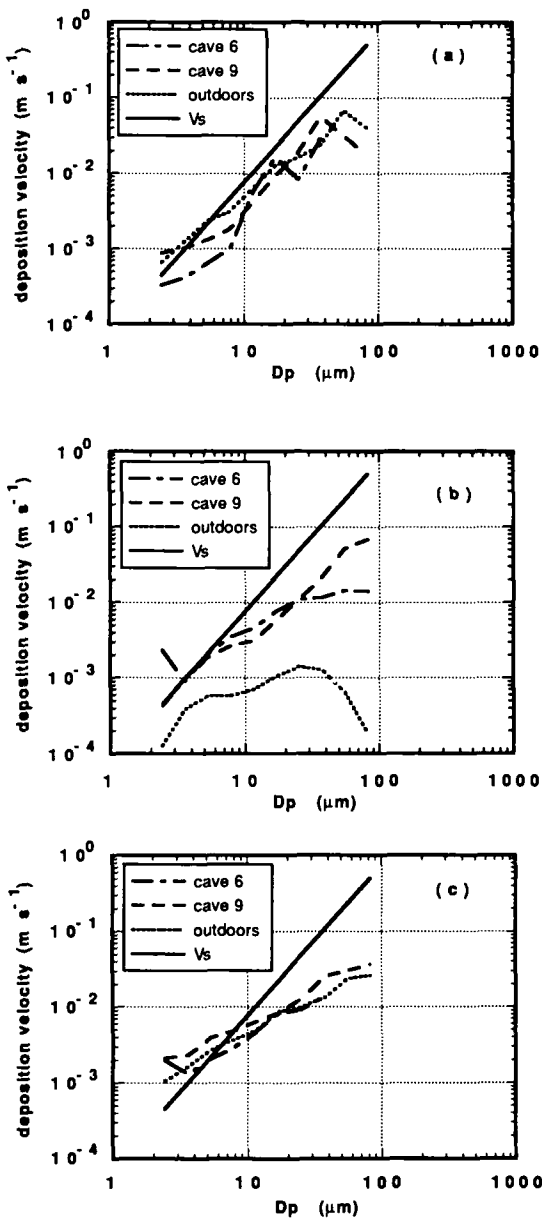


Fig. 7. Deposition velocity onto horizontal surfaces at Yungang as a function of particle diameter d_p (dashed lines) compared to the terminal gravitational settling velocity, V_s , of equivalently sized spherical particles of density 2.2 g cm^{-3} (solid line): (a) 14 April, 1991, (b) 1 May, 1993, (c) spring average, 1991.

the spring is warmer than the cave walls during the day but colder at night, and natural convection driven flows reverse direction in a regular diurnal pattern.

Over the period 29 April–1 May 1991, strong wind storms occurred at Yungang, with wind speeds at times exceeding 8 m s^{-1} , accompanied by coarse airborne particle concentrations exceeding $1200 \mu\text{g m}^{-3}$ over a 24 h averaging time on 1 May. The largest deviation between the terminal settling velocity curves

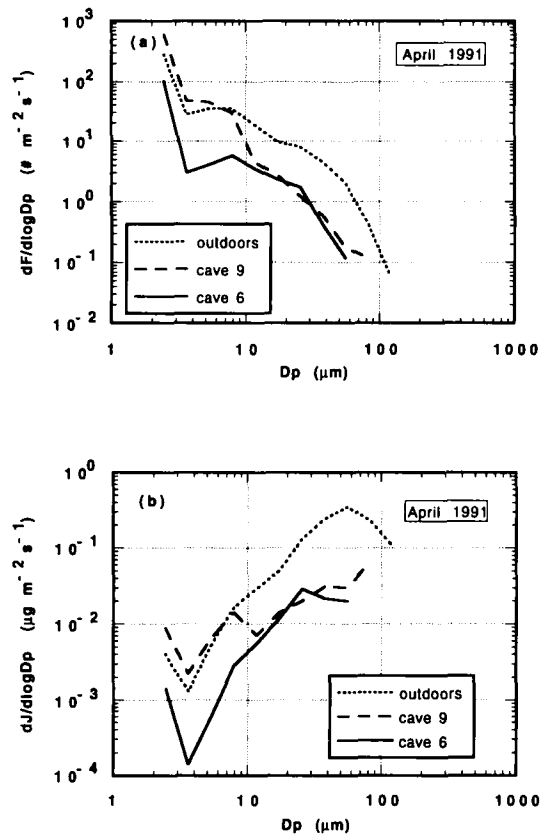


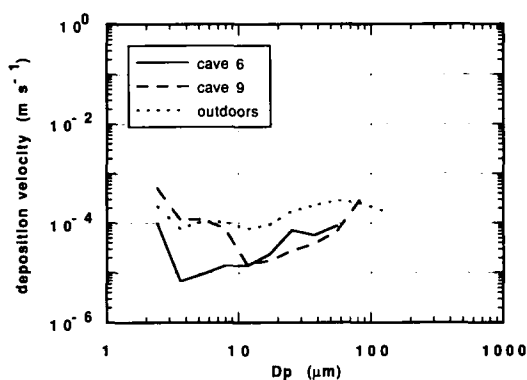
Fig. 8. Coarse particulate matter deposited onto vertical surfaces at Yungang, April 1991, as a function of particle diameter d_p : (a) average number flux, F , and (b) average mass flux, J .

and the experimental values occurs in the larger size intervals during such high-wind events as shown in Fig. 7b. That result is due to scouring of the larger coarse particles by wind gusts outdoors (the deposition plates were ungreased because we wished to mimic the ungreased statuary). When averaging over the course of a month, events like those shown in Fig. 7b reduce the apparent net deposition velocity for larger coarse particles, yielding a spring seasonal average like that of Fig. 7c. The deposition velocity curves might also be affected by the fact that there are not many particles to be counted in the largest size intervals and therefore results are prone to a higher degree of uncertainty at the largest particle sizes.

Deposition measurements to vertical surfaces during the spring sampling period are presented in Table 6 and Fig. 8a, b. Data on the deposition velocity as a function of particle size to vertical surfaces are exceedingly sparse. Ligocki *et al.* (1990) have reported fine particle deposition velocity measurements to vertical surfaces from a study conducted inside museums. In a related but different context, Liu and Ahn (1987) have reported on particle deposition rates onto silicon wafers inside laminar flow clean rooms used during the manufacture of semiconductor devices. One of the

Table 6. Average projected surface area flux of coarse particulate matter onto vertical surfaces at Yungang, April 1991

Size interval (μm)	Outdoors ($\mu\text{m}^2 \text{m}^{-2} \text{s}^{-1}$)	Cave 9 ($\mu\text{m}^2 \text{m}^{-2} \text{s}^{-1}$)	Cave 6 ($\mu\text{m}^2 \text{m}^{-2} \text{s}^{-1}$)
2.02–2.99	220	480	83
3.00–4.42	48	83	5
4.43–6.54	130	170	16
6.55–9.67	290	250	48
9.68–14.2	340	81	64
14.3–21.1	390	110	93
21.2–31.2	700	110	150
31.3–46.2	870	110	78
46.3–68.4	850	73	49
68.5–101.2	380	110	—
101.3–149.7	120	—	—
Total	4340	1580	590

Fig. 9. Deposition velocity onto vertical surfaces at Yungang, Spring 1991 as a function of particle diameter d_p .

reasons that data are seldom available for coarse particle deposition as a function of particle size onto vertical surfaces is that the flux of coarse particles towards a vertical surface is very small. As a result, long sampling times are required if measurements are to be made. In the case of the present study at Yungang, the sample collection lasted for the entire duration of the spring experiment (a little less than 19 d). Even so, there were not many particles present, especially in the larger size intervals. Figure 9 shows the deposition velocity for particles depositing onto vertically oriented smooth surfaces. It can be seen that the deposition velocity values range from 10^{-3} to 10^{-5} m s^{-1} . The surface area coverage rate on vertical surfaces shown in Table 6 is two orders of magnitude lower than for coarse particle deposition to horizontal surfaces, and confirms that the soiling problem should be (and is) most evident on upward facing surfaces inside the caves. The outdoor deposition velocity curve remains almost flat with increasing particle diameter. Ligocki *et al.* (1990) provide deposition velocity graphs for fine particle ($d_p < 2.1 \mu\text{m}$) accumulation on smooth vertical surfaces. It is seen that the

trend there is the same, i.e. particle deposition velocity remains almost constant over the range of particle diameters studied.

CONCLUSIONS

Coarse particle deposition rates onto horizontal surfaces have been measured as a function of particle size at the Yungang Grottoes. The mass fluxes were found to range from $13.42 \mu\text{g m}^{-2} \text{s}^{-1}$ outdoors to $5.23 \mu\text{g m}^{-2} \text{s}^{-1}$ inside Cave 6 over a 1 yr period. These mass deposition rates are approximately the same as estimates derived by removal of historically accumulated deposits from within the caves. Size distribution measurements show that most of the deposited mass is contributed by particles larger than 20–30 μm in diameter.

The rate of surface area coverage by coarse particles depositing on horizontal surfaces inside the caves was measured, and ranged from $2.9 \times 10^5 \mu\text{m}^2 \text{m}^{-2} \text{s}^{-1}$ inside Cave 9 to $1.2 \times 10^5 \mu\text{m}^2 \text{m}^{-2} \text{s}^{-1}$ inside Cave 6. At a surface area coverage rate of $2 \times 10^5 \mu\text{m}^2 \text{m}^{-2} \text{s}^{-1}$, 100% surface coverage by deposited particles occurs within a two month period, clearly explaining why the statues inside the caves are becoming visibly soiled at a rapid rate.

Measurements show that there is a marked decrease in the deposition of coarse particles inside Cave 6 when compared to Cave 9 and the outdoors. Also, mass deposition rates inside Cave 6 were found to be almost constant over the course of a year. That might be attributed to the wooden temple front structure that protects the entrance to Cave 6 and that acts as a partial barrier to the migration of particles from the outside. Cave 9 has no such temple front, and clearly a greater fraction of the outdoor particles enter Cave 9. Reconstruction of wooden temple fronts over the entrances to the remaining caves thus would be expected to slow the soiling problem somewhat. If careful thought is given to the design, even better

protection than is presently provided by the shelter over Cave 6 could be achieved through installation of an air filtration system within existing or reconstructed temple front buildings (Nazaroff and Cass, 1991). The particle concentration and size distribution data reported here should facilitate the design of such a particle control system.

Acknowledgements—This work is supported by a research agreement from the Getty Conservation Institute (GCI). The co-operation and assistance of the staff of the Yungang Grottoes and the State Bureau of Cultural Relics, Beijing is gratefully acknowledged including Huang Kezhong, Zhu Changling, Sheng Weiwei, Li Xiu Qing, Li Hua Yuan, Xie Ting Fan, Yuan Jin Hu, Huang Ji Zhong, Zhi Xia Bing, Bo Guo Liang of the Shanxi Institute of Geological Science, and Zhong Ying from Taiyuan University. Assistance critical to this work was provided by the Getty Conservation Institute and their consultants, and we especially thank Neville Agnew, Po-Ming Lin, Shin Maekawa, and Roland Tseng for their help.

REFERENCES

- Cox L. B. (1957) *The Buddhist Cave-Temples of Yün-Kang & Lung-Men*. The Australian National University, Canberra, Australia.
- Flagan R. C. and Seinfeld J. H. (1988) *Fundamentals of Air Pollution Engineering*. Prentice Hall, New Jersey, U.S.A.
- Hancock R. P., Esmen N. A. and Furber C. P. (1976) Visual response to dustiness. *J. Air Pollut. Control Ass.* **26**, 54–57.
- Heidenreich E. (1987) Particle characterization by size and shape. *J. Aerosol Sci.* **18**, 777–780.
- John W., Fritter D. N. and Winklmayr W. (1991) Resuspension induced by impacting particles. *J. Aerosol Sci.* **22**, 723–736.
- Knauer E. R. (1983) The fifth century A.D. Buddhist cave temples at Yün-Kang, North China. *Expedition, summer*, 27–47.
- Ligocki M. P., Liu H. I. H., Cass G. R. and John W. (1990) Measurements of particle deposition rates inside Southern California museums. *Aerosol Sci. Technol.* **13**, 85–101.
- Liu B. Y. H. and Ahn K. (1987) Particle deposition on semiconductor wafers. *Aerosol Sci. Technol.* **6**, 215–224.
- Nazaroff W. W. and Cass G. R. (1989a) Mass-transport aspects of pollutant removal at indoor surfaces. *Envir. Int.* **15**, 567–584.
- Nazaroff W. W. and Cass G. R. (1989b) Mathematical modeling of indoor aerosol dynamics. *Envir. Sci. Technol.* **23**, 157–166.
- Nazaroff W. W. and Cass G. R. (1991) Protecting museum collections from soiling due to the deposition of airborne particles. *Atmospheric Environment* **25A**, 841–852.
- Nicholson K. W. (1988) The dry deposition of small particles: a review of experimental measurements. *Atmospheric Environment* **22**, 2653–2666.
- Salmon L. G., Christoforou C. S. and Cass G. R. (1994) Airborne pollutants in the Buddhist cave temples at the Yungang Grottoes, China. *Envir. Sci. Technol.* (in press).
- Sehmel G. A. (1980) Particle and gas dry deposition: a review. *Atmospheric Environment* **14**, 983–1011.